

# Electromagnetic calorimeters based on scintillating lead tungstate crystals for experiments at Jefferson Lab <sup>☆</sup>

A.Asaturyan<sup>a</sup>, F.Barbosa<sup>c</sup>, V.Berdnikov<sup>b</sup>, J.Crafts<sup>b,c</sup>, H.Egiyan<sup>c</sup>, L.Gan<sup>f</sup>, A.Gasparian<sup>g</sup>, K.Harding<sup>c</sup>, T.Horn<sup>b</sup>, V.Kakoyan<sup>a</sup>, H.Mkrtchyan<sup>a</sup>, Z.Papandreou<sup>e</sup>, V. Popov<sup>c</sup>, N.Sandoval<sup>c</sup>, A.Somov<sup>c,\*</sup>, S.Somov<sup>d</sup>, A. Smith<sup>h</sup>, C. Stanislav<sup>c</sup>, S.Taylor<sup>c</sup>, H. Voskanyan<sup>a</sup>, T. Whitlatch<sup>c</sup>, S. Worthington<sup>c</sup>

<sup>a</sup>A. I. Alikhanian National Science Laboratory (Yerevan Physics Institute), 0036 Yerevan, Armenia

<sup>b</sup>Catholic University of America, Washington, DC 20064, USA

<sup>c</sup>Thomas Jefferson National Accelerator Facility, Newport News, VA 23606, USA

<sup>d</sup>National Research Nuclear University MEPhI, Moscow 115409, Russia

<sup>e</sup>University of Regina, Regina, Saskatchewan, Canada S4S 0A2

<sup>f</sup>University of North Carolina at Wilmington, Wilmington, NC 28403, USA

<sup>g</sup>North Carolina A&T State University, Greensboro, NC 27411, USA

<sup>h</sup>Duke University, Durham, NC 27708, USA

## Abstract

A new electromagnetic calorimeter consisting of 140 lead tungstate (PbWO<sub>4</sub>) scintillating crystals was constructed for the PrimEx  $\eta$  experiment at Jefferson lab. The calorimeter was integrated into the data acquisition and trigger systems of the GlueX detector and used in the experiment to reconstruct Compton scattering events. The experiment started collecting data in the spring of 2019 and acquired about 30% of the required statistics. The calorimeter is a prototype for two PbWO<sub>4</sub>-based detectors: the Neutral Particle Spectrometer (NPS) and the lead tungstate insert of the forward calorimeter (FCAL) of the GlueX detector. The article presents the design and performance of the Compton calorimeter and gives a brief overview of the FCAL and NPS projects.

**Keywords:** Electromagnetic calorimeter, Lead tungstate scintillator

## 1. Introduction

Electromagnetic calorimeters based on PbWO<sub>4</sub> scintillating crystals have a widespread application in experiments at different accelerator facilities such as CERN, FNAL, GSI, and Jefferson Lab (JLab). The small radiation length ( $L_R = 0.89$  cm) and Molière radius ( $R_M = 2.19$  cm) of PbWO<sub>4</sub> allows to build high-granularity detectors with a good spatial separation and energy resolution of reconstructed electromagnetic showers, which makes these crystals the material of choice in many of these applications.

Two electromagnetic calorimeters are currently under construction in experimental Hall D and Hall C at Jefferson Lab, both using rectangular 2.05 cm  $\times$  2.05 cm  $\times$  20 cm PbWO<sub>4</sub> scintillating modules. The inner part of the forward lead glass calorimeter of the GlueX detector [1] in Hall D will be upgraded with these high-granularity, high-resolution crystals. This upgrade is required by the physics program with the GlueX detector, specifically the new experiment to study rare decays of  $\eta$  mesons [2]. The Neutral Particle Spectrometer [3] in experimental Hall C consists of a PbWO<sub>4</sub> electromagnetic calorimeter

preceded by a sweeping magnet. The NPS is required by Hall C's precision cross section measurement program with neutral final states [4–9]. Such precision measurements of small cross sections play a central role in studies of transverse spatial and momentum hadron structure. The NPS detector consists of 1080 PbWO<sub>4</sub> crystals arranged in a 30  $\times$  36 array. Lead tungstate crystals for both detectors were procured from two vendors: Shanghai Institute of Ceramics (SICCAS) in China and CRYTUR in the Czech Republic. The quality of recently produced PbWO<sub>4</sub> scintillators has been studied in detail by the NPS and EIC eRD1 collaborations and is described in Ref. [10]. PbWO<sub>4</sub> crystals are also being considered for an electromagnetic calorimeter of the future Electron-Ion Collider [11].

In this article we describe the design and construction of a calorimeter prototype composed of 140 SICCAS crystals, which served as the Compton Calorimeter (CCAL) in the PrimEx  $\eta$  experiment [12] with the GlueX detector in the spring of 2019. The CCAL was subsequently used during a few short GlueX physics runs at high luminosity in order to study rates and operating conditions expected for the FCAL lead-tungstate insert. Experience gained during fabrication and operation of the CCAL was critical for finalizing the design of the FCAL insert and also helped further optimize the NPS calorimeter.

This article is organized as follows: we will present the PrimEx  $\eta$  experiment and performance of the CCAL in Section 2 and Section 3, and will briefly describe the FCAL and NPS projects in Sections 4 and 5.

<sup>☆</sup>Notice: Authored by Jefferson Science Associates, LLC under U.S. DOE Contract No. DE-AC05-06OR23177. The U.S. Government retains a non-exclusive, paid-up, irrevocable, world-wide license to publish or reproduce this manuscript for U.S. Government purposes.

\*Corresponding author. Tel.: +1 757 269 5553; fax: +1 757 269 6331.

Email address: somov@jlab.org (A.Somov)

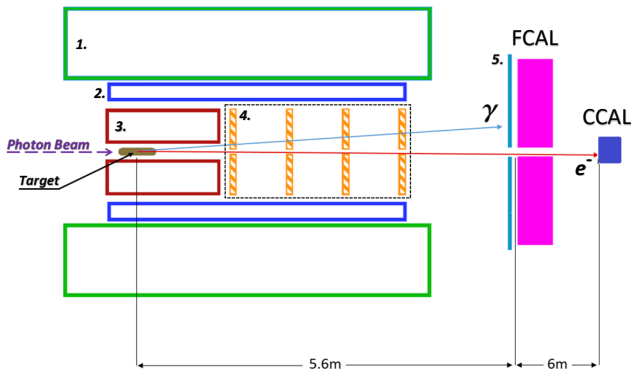


Figure 1: Schematic layout of the GlueX detector (not to scale). Numbers represent the following detector components: solenoid magnet (1), barrel calorimeter (2), central drift chamber (3), forward drift chambers (4), time-of-flight wall (5).

## 2. PrimEx $\eta$ experiment with the GlueX detector

The GlueX detector [1] was designed to perform experiments using a photon beam. Beam photons are produced via the bremsstrahlung process by electrons, provided by the JLab electron accelerator facility, incident on a thin radiator. The energy of a beam photon ( $E_\gamma$ ) is determined by detecting a scattered electron after radiating the photon as follows:  $E_\gamma = E_e - E'_e$ , where  $E_e$  is the primary electron beam energy and  $E'_e$  is the energy of the bremsstrahlung electron. The bremsstrahlung electron is deflected in a 6 m long dipole magnet operated at a field of 1.8 T and registered in the so-called tagging scintillator counters. Each counter corresponds to the specific energy of the reconstructed lepton. The tagging detectors span the beam photon energy range between 25% and 98% of the electron beam energy and covered the range between 2.8 GeV and 11.0 GeV during the PrimEx  $\eta$  experiment<sup>1</sup>. The typical energy resolution of the beam photon is 0.1 – 0.2%. The photon beam propagates toward the GlueX target. A schematic view of the GlueX detector is illustrated in Fig. 1<sup>2</sup>.

The physics goal of the PrimEx  $\eta$  experiment is to perform a precision measurement of the  $\eta \rightarrow \gamma\gamma$  decay width. The measurement will provide an important test of quantum chromodynamics symmetries and is essential for the determination of fundamental properties such as the ratios of the light quark masses and the  $\eta$ - $\eta'$  mixing angle. The decay width will be extracted from the measurement of the photoproduction cross section of  $\eta$  mesons in the Coulomb field of a nucleus, which is known as the Primakoff effect. The  $\eta$  mesons will be reconstructed by

<sup>1</sup>The electron beam energy during most production PrimEx  $\eta$  runs was 11.2 GeV.

<sup>2</sup>Not shown on this plot is the DIRC detector, which was installed after the PrimEx  $\eta$  experiment and is used for the particle identification in the forward direction.

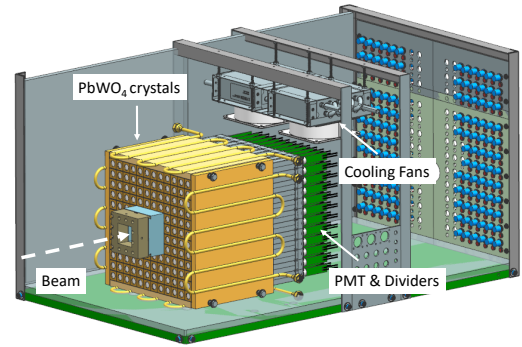


Figure 2: Schematic layout of the Compton calorimeter.

detecting two decay photons in the forward calorimeter of the GlueX detector.

The cross section will be normalized using the Compton scattering process, which will also be used to monitor the luminosity and control the detector stability during data taking. Electrons and photons originating from Compton events in the target are produced at small angles, typically outside the acceptance of the FCAL. In order to improve the reconstruction of particles in the forward direction, we built a small Compton calorimeter consisting of 140 lead tungstate scintillating crystals and positioned it about 6 m downstream from the FCAL as shown in in Fig. 1. The CCAL covers the angular range between  $0.19^\circ$  and  $0.47^\circ$ .

The PrimEx  $\eta$  experiment started collecting data in the spring of 2019 and has acquired 30% of the required statistics. During the experiment, the magnetic field of the solenoid magnet was switched off in order to allow reconstruction of Compton events. The photon flux was about  $5 \cdot 10^6 \gamma/\text{sec}$  (about five times lower than the nominal GlueX flux) in the beam energy range of interest between 9.5 GeV and 11.6 GeV.

## 3. Compton calorimeter of the PrimEx $\eta$ experiment

### 3.1. Calorimeter design

The calorimeter design is shown in Fig. 2. The CCAL comprises an array of  $12 \times 12$  lead tungstate modules with a  $2 \times 2$  hole in the middle for the passage of the photon beam. The modules are positioned inside a light tight box. A tungsten absorber is placed in front of the innermost layer closest to the beamline to provide protection from the high rate of particles predominantly originating from electromagnetic interactions.

The light yield from  $\text{PbWO}_4$  crystals depends on temperature with a typical coefficient of  $2\%/^\circ\text{C}$  at room temperature. Maintaining constant temperature is essential for the calorimeter operation. The calorimeter modules are surrounded by four copper plates with built-in pipes to circulate a cooling liquid and provide temperature stabilization. Foam insulation surrounds the detector box. The temperature was monitored and recorded during the experiment by five thermocouples attached to different points of the  $\text{PbWO}_4$  module assembly. During the experi-

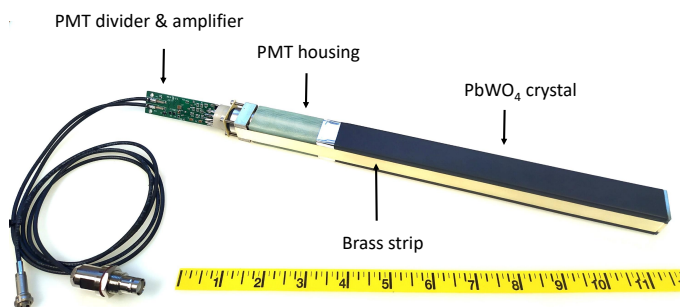


Figure 3: Calorimeter module showing main components: the PbWO<sub>4</sub> crystal, PMT housing, PMT divider, and signal and high-voltage cables.

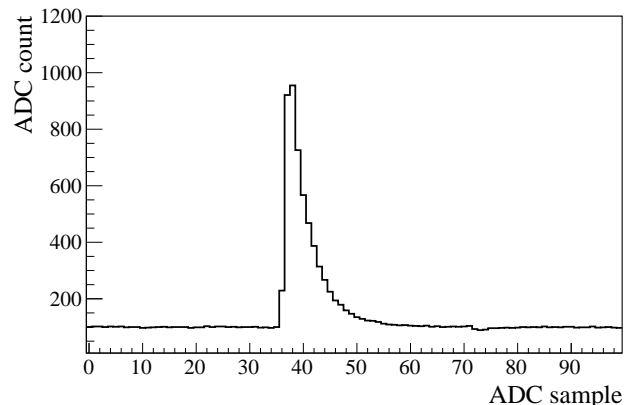


Figure 4: A typical flash ADC signal pulse obtained from a PbWO<sub>4</sub> module.

114 ment the temperature was maintained at  $17^\circ \pm 0.2^\circ\text{C}$ . The typ-  
 115 ical heat released by the photomultiplier tube (PMT) dividers  
 116 was equivalent to about 30 Watts. In order to prevent condensa-  
 117 tion, a nitrogen purge was applied. Two fans with a water-based  
 118 cooling system were installed on the top of the crystal assem-  
 119 bly to improve nitrogen circulation and heat dissipation from  
 120 the PMT dividers. The detector was positioned on a platform,  
 121 which allowed to move it in the vertical and horizontal direc-  
 122 tions, perpendicular to the beam. The platform was remotely  
 123 controlled and provided a position accuracy of about  $200\ \mu\text{m}$ .  
 124 During detector calibration each module was moved into the  
 125 beam.

### 126 3.2. Module design

127 The design of the PbWO<sub>4</sub> module is based on the HyCal  
 128 calorimeter, which was used in several experiments in Jeffer-  
 129 son Lab Hall B [13, 14]. An assembled calorimeter module  
 130 is presented in Fig. 3. Each lead tungstate crystal is wrapped  
 131 with a  $60\ \mu\text{m}$  polymer Enhanced Specular Reflector film (ESR)  
 132 manufactured by 3M<sup>TM</sup>, which allows 98.5% reflectivity across  
 133 the visible spectrum. In order to improve optical isolation of  
 134 each module from its neighbors, each crystal is wrapped with a  
 135 layer of  $25\ \mu\text{m}$  thick Tedlar. The PMT is located inside a G-10  
 136 fiberglass housing at the rear end of the crystal. Two flanges are  
 137 positioned at the crystal and housing ends and are connected to-  
 138 gether using  $25\ \mu\text{m}$  brass straps, which are brazed to the sides  
 139 of the flanges. Four set screws are pressed to the PMT housing  
 140 flange to generate tension in the straps and hold the assembly  
 141 together. Light from the crystal is detected using a ten-stage  
 142 Hamamatsu PMT 4125, which is inserted into the housing and  
 143 is coupled to the crystal using optical grease (EJ-550). The  
 144 PMT diameter is 19 mm. The PMT is pushed towards the crys-  
 145 tal by using a G-10 retaining plate attached to the back of the  
 146 PMT and four tension screws applied to the PMT flange. The  
 147 PMT is instrumented with a high-voltage (HV) divider and am-  
 148 plifier positioned on the same printed circuit board attached to  
 149 the PMT socket.

### 3.3. Electronics

160 The PMT of each calorimeter module was equipped with an  
 161 active base prototype [15], which was designed for the Neutral  
 162 Particle Spectrometer in experimental Hall C. The base com-  
 163 bines a voltage divider and an amplifier powered by the current  
 164 flowing through the divider. The active base allows the opera-  
 165 tion of the PMT at lower voltage and consequently at lower  
 166 anode current, which improves the detector rate capability and  
 167 prolongs the PMT's life. The original Hamamatsu divider for  
 168 this type of PMT was modified by adding two bipolar transis-  
 169 tors on the last two dynodes, which provides gain stabilization  
 170 at high rate. The active base has a relatively large amplification  
 171 of about a factor of 24 due to the large PMT count rate pre-  
 172 dicted by Monte Carlo simulation of the NPS detector. Large  
 173 amplification was not needed for the planned run conditions  
 174 of the PrimEx  $\eta$  experiment. However, we subsequently used  
 175 CCAL in GlueX runs at significantly larger luminosity in order  
 176 to study run conditions of the FCAL lead tungstate insert,  
 177 where the amplifier will be required. This will be discussed in  
 178 Section 4.0.3. During the PrimEx run, the CCAL PMTs were  
 179 operated at about 680 V, which produced a divider current of  
 180  $260\ \mu\text{A}$ . The high voltage for each PMT was supplied by a  
 181 24-channel CAEN A7236SN module positioned in a SY4527  
 182 mainframe.

183 Amplified PMT signals were digitized using a twelve-bit 16-  
 184 channel flash ADCs electronics module operated at a sampling  
 185 rate of 250 MHz. The ADC was designed at Jefferson Lab [16]  
 186 and is used for the readout of several sub-detectors of the GlueX  
 187 detector. The Field-Programmable Gate Array (FPGA) chip  
 188 inside the ADC module allows the implementation of various  
 189 programmable data processing algorithms for the trigger and  
 190 readout. An example of a flash ADC signal pulse obtained  
 191 from a calorimeter module is shown in Fig. 4. In this exam-  
 192 ple, the ADC is operated in the raw readout mode, where digi-  
 193 tized amplitudes are read out for 100 samples, corresponding  
 194 to the read out window size of 400 ns. During the PrimEx  $\eta$   
 195 experiment, the ADC performed on-board integration of signal  
 196 pulses, which amplitudes were above a threshold of 24 MeV.  
 197 Amplitudes were summed in a time window of 64 ns and read

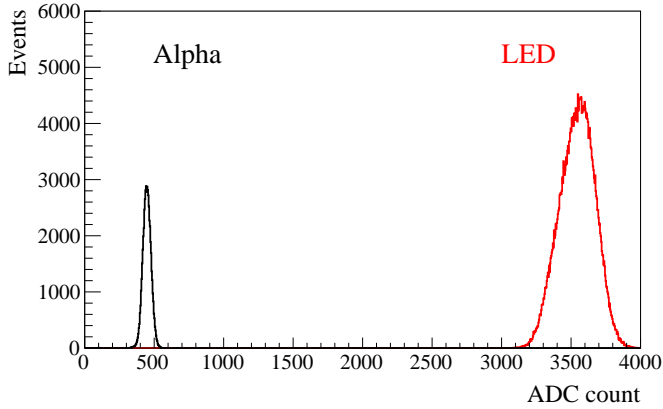


Figure 5: Flash ADC signal amplitudes induced by the LED and  $\alpha$ -source in the reference PMT.

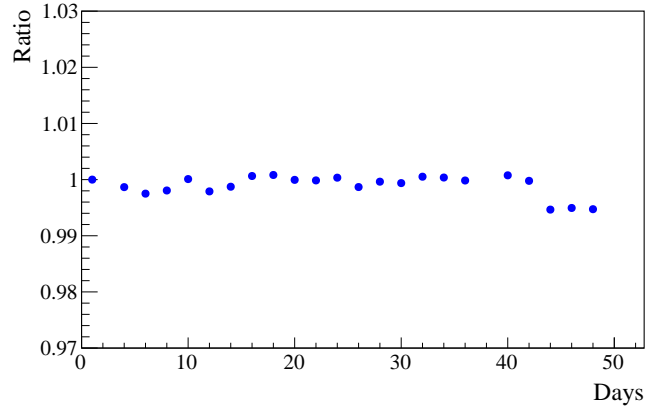


Figure 6: Ratio of signal ADC amplitudes from the LED pulser to the  $\alpha$ -source measured by the reference PMT during different run periods of the 48-day long PrimEx  $\eta$  experiment. The ratio is normalized to data in the beginning of the run.

189 out from the ADC module along with other parameters such  
 190 as the pulse peak amplitude, pulse time, and data processing  
 191 quality factors. This readout mode allowed to significantly re-  
 192 duce the data size and ADC readout time, and therefore did not  
 193 induce any dead time in the data acquisition.

194 CCAL flash ADCs are positioned in a VXS (ANSI/VITA  
 195 41.0 standard) crate. VXS crates are used to host all readout  
 196 electronics of the GlueX experiment. In addition to the VME-  
 197 bus used to read out data from electronics modules, the VXS is  
 198 instrumented with a high-speed serial bus in order to increase  
 199 the bandwidth to several Gb/sec and provide an interconnected  
 200 network between modules. The bus is used to transmit ampli-  
 201 tudes digitized by the ADC to trigger electronics modules to  
 202 include the CCAL in the Level 1 trigger system of the GlueX  
 203 detector.

### 3.4. Light Monitoring System

204 To monitor performance of each calorimeter channel, we  
 205 designed an LED-based light monitoring system (LMS). The  
 206 LMS optics includes a blue LED, a spherical lens to correct  
 207 the conical dispersion of the LED, and a diffusion grating to  
 208 homogeneously mix the light. Light produced by the LED is  
 209 incident on a bundle of plastic optical fibers (Edmund Optics)  
 210 with a core diameter of 250  $\mu\text{m}$ . Each fiber distributes light to  
 211 an individual calorimeter module. On the crystal end, the fiber  
 212 is attached to the module using a small acrylic cap glued to the  
 213 crystal with a hole drilled through each cap to hold the fiber  
 214 inside.

215 To monitor stability of the LED, we used two reference  
 216 Hamamatsu 4125 PMTs, the same type as in the CCAL detec-  
 217 tor. Each PMT receives light from two sources: a single fiber  
 218 from the LED and a YAP:Ce pulser unit, both glued to the PMT  
 219 face. The pulser unit consists of a 0.15 mm thick YAP:Ce scin-  
 220 tillation crystal with a diameter of 3 mm spot activated by an  
 221  $^{241}\text{Am}$   $\alpha$  source. The  $\alpha$  source is used to monitor stability of  
 222 the LED. The PMT was read out using a flash ADC. The high  
 223 voltage on each reference PMT was adjusted to have the sig-  
 224 nals from both the LED and  $\alpha$  source fit within the range of

12-bit flash ADC corresponding to 4096 counts, as shown in  
 Fig. 5. Each LED was driven by a CAEN 1495 module, which  
 allowed to generate LED pulses with a programmable rate. The  
 LMS was integrated into the GlueX trigger system and provided  
 a special trigger type during data taking. The LMS was ex-  
 tensively used during the detector commissioning and injected  
 light to the CCAL detector with a typical frequency of 100 Hz  
 continuously during the PrimEx  $\eta$  experiment. This LED rate  
 is similar to the trigger rate of events produced by the reference  
 $\alpha$  source.

238 Most LMS components were positioned inside the  
 239 temperature-stabilized detector box. The stability of the  
 240 LED system measured using the reference PMTs during the  
 241 entire PrimEx run was on the level of 1%. The ratio of signal  
 ADC amplitudes from the LED pulser to the  $\alpha$  source obtained  
 during different run periods of the 48-day long PrimEx  $\eta$   
 experiment is presented in Fig. 6. The ratio is normalized  
 to the data in the beginning of the experiment. Stability of  
 most CCAL modules observed using the LMS during the  
 experiment was better than 6%. We did not apply any PMT  
 gain adjustments during the experiment.

### 3.5. Calibration

The initial energy calibration of the CCAL was performed  
 by moving the calorimeter platform and positioning each mod-  
 ule into the photon beam during special low-intensity calibra-  
 tion runs. The maximum rate in the module exposed to the  
 beam did not exceed 200 kHz at a threshold of 15 MeV. The  
 energy of each beam photon was determined by detecting a  
 bremsstrahlung electron using the GlueX tagging detectors de-  
 scribed in Section 2. The spot size of the collimated photon  
 beam had a diameter of about 6 mm.

In the beginning of the calibration run, we adjusted the PMT  
 high voltage for each module in order to equalize signal pulse  
 amplitudes induced by 11 GeV beam photons. The amplitude  
 was set to 3500 ADC counts, which corresponds to  $\sim 1.7$  V. An

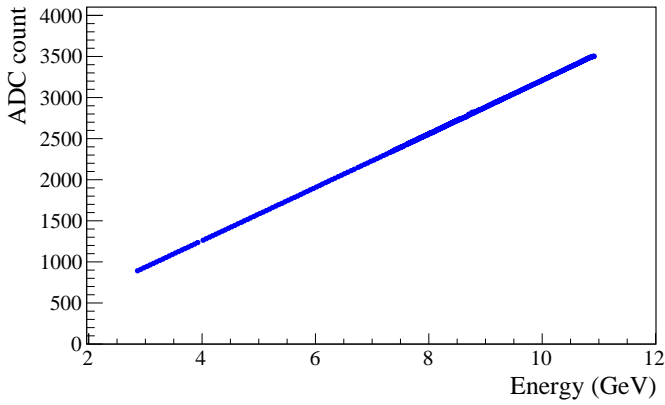


Figure 7: ADC signal pulse amplitude in the CCAL module as a function of the beam energy.

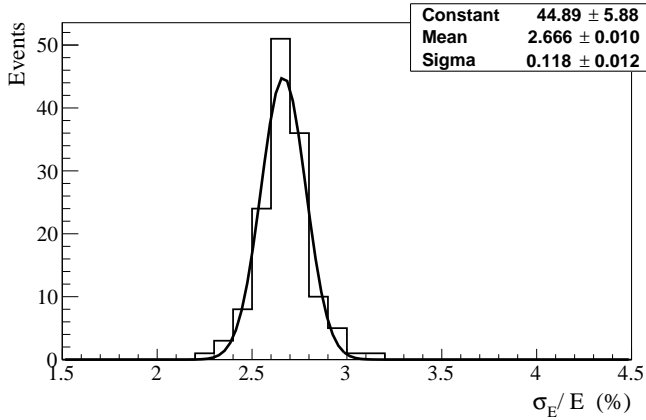


Figure 8: Relative energy resolution of 140 PbWO<sub>4</sub> modules installed on the CCAL measured with 6 GeV beam photons.

example of flash ADC signal amplitude in the calorimeter module as a function of the beam energy is presented in Fig. 7. The calibration of each module was refined by reconstructing showers in the calorimeter and constraining the reconstructed energy to the known beam energy.

During the calibration runs, we estimated the non-uniformity of the 140 CCAL modules by measuring the relative energy resolution for each individual module exposed to the beam. The energy resolution obtained for 6 GeV photons is presented in Fig. 8. The distribution is fit to a Gaussian function. The non-uniformity of the modules, i.e., the spread of the distribution is found to be smaller than 5%.

During calibration, we observed some non-linearity of the PMT active base with the large amplification factor of 24, on the level of a few percent, which impacted both the pulse peak and pulse integral. The base performance became linear when the amplifier gain was reduced. In order to study the impact of the non-linearity on the detector energy resolution, we replaced the original PMT active bases for 9 CCAL modules (in the array of 3 × 3 modules) with modified bases where the amplifier was bypassed. After adjusting high voltages and recalibrating PMT

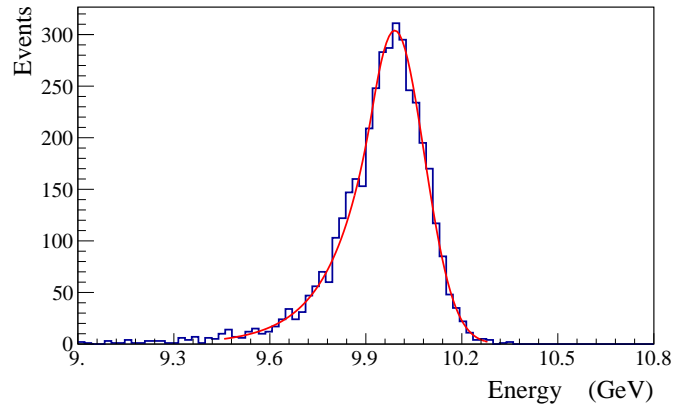


Figure 9: Energy distribution deposited by 10 GeV beam photons. The spectrum is fit to a Crystal Ball function.

gains, we measured the energy resolution for different beam energies. The beam was incident on the center of the middle module in the array. An example of the energy deposited by 10 GeV photons is shown in Fig. 9. The energy resolution was obtained from a fit of the energy distribution to a Crystal Ball function<sup>3</sup> implemented in the ROOT data analysis framework [17]. The energy resolution as a function of the beam energy is shown in Fig. 10. The distribution was fit to the following function:

$$\frac{\sigma_E}{E} = \frac{S}{\sqrt{E}} \oplus \frac{N}{E} \oplus C, \quad (1)$$

where  $S$  represents the stochastic term,  $N$  the electronic noise and  $C$  the constant term,  $E$  is the beam energy in GeV, and the symbol  $\oplus$  indicates a quadratic sum. The fit yields:  $S = 2.63 \pm 0.01\%$ ,  $N = 1.07 \pm 0.09\%$ , and  $C = 0.53 \pm 0.01\%$ . The resolution was found to be about 10% better than that measured with the original base with the amplifier gain of 24<sup>4</sup>. The energy resolution is consistent with that of the HyCal calorimeter [13], which was instrumented with crystals produced by SICCAS in 2001 and was used in several experiments in Jefferson Lab's experimental Hall B. The HyCal PbWO<sub>4</sub> crystals have the same transverse size of 2.05 cm × 2.05 cm, but a smaller length of 18 cm. The initial CCAL calibration performed with the beam scan was fine-tuned after the PrimEx  $\eta$  run by using showers of reconstructed Compton scattering candidates and constraining the reconstructed energy in the event to the known beam energy.

### 3.6. Performance during the PrimEx $\eta$ run

In the PrimEx  $\eta$  experiment, we reconstruct Compton events produced by beam photons with the energy larger than 6 GeV. This energy range is covered by the GlueX pair spectrometer [18], which determines the photon flux needed for cross section measurements. An electron and photon produced in

<sup>3</sup>The function is named after the Crystal Ball collaboration.

<sup>4</sup>The linearity of the PMT active base is being currently improved; modified active bases will be installed before the new PrimEx  $\eta$  run in 2021.



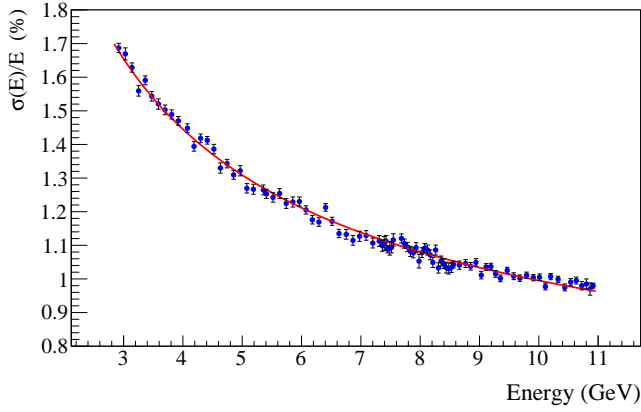


Figure 10: Energy resolution as a function of the photon energy.

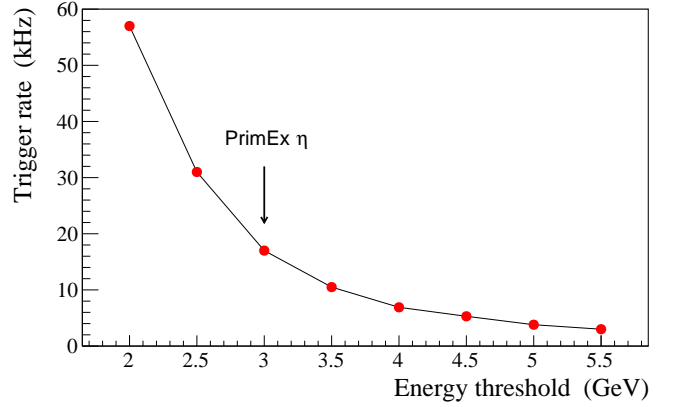


Figure 11: Trigger rate as a function of the total energy deposited in the FCAL and CCAL. The arrow indicates the energy threshold used in PrimEx  $\eta$  production runs.

313 the Compton scattering process were detected by reconstruct-  
 314 ing two showers, one in the FCAL and another one in the 352  
 315 CCAL. The event topology of the reaction is such that the 353  
 316 more energetic electron predominantly goes into the Compton 354  
 317 calorimeter, while the photon strikes the FCAL. In order 355  
 318 to accept Compton events during data taking and to reduce 356  
 319 background originating from low-energy electromagnetic and 357  
 320 hadronic interactions, the CCAL was integrated to the Level 1 358  
 321 trigger system of the GlueX detector. The physics trigger was 359  
 322 based on the total energy deposited in the forward and Compton 360  
 323 calorimeters. The GlueX trigger is implemented on special- 361  
 324 purpose programmable electronics modules with FPGA chips. 362  
 325 The trigger architecture is described in Ref. [19]. The trigger 363  
 326 rate as a function of the energy threshold is presented in Fig. 11. 364  
 327 We collected data using a relatively small energy threshold of 365  
 328 3 GeV at a trigger rate of about 18 kHz. This rate did not pro- 366  
 329 duce any dead time in the data acquisition and trigger systems. 367  
 330 The trigger rate was reproduced by a detailed Geant detector 368  
 331 simulation. 369

332 The rate in the CCAL modules during the experiment is pre- 370  
 333 sented in Fig. 12. In this plot, the photon beam goes through the 371  
 334 center of the hole of  $2 \times 2$  modules in the middle of the detec- 372  
 335 tor. The rate is the largest in innermost detector layers closest 373  
 336 to the beam line. The maximum rate in the detector module 374  
 337 was about 200 kHz for an energy threshold of 30 MeV, which 375  
 338 is equivalent to a signal pulse amplitude of 5 mV. Before the 376  
 339 experiment, we performed a high-rate performance study of the 377  
 340 PMT and electronics using a laser and an LED pulser and did 378  
 341 not find any degradation of the PMT gain up to 2-3 MHz [20]. 379

342 Timing resolution of reconstructed showers is an important 380  
 343 characteristic of the detector performance. In the experiment 381  
 344 we used timing information provided by the calorimeters to 382  
 345 identify the accelerator beam bunch for which the interaction 383  
 346 occurred in the detector and therefore relate showers in the 384  
 347 calorimeters with hits in the tagging detector, from the same 385  
 348 event. A hit in the tagging detector defines the energy of the 386  
 349 beam photon. The time in the calorimeter module is provided 387  
 350 by an algorithm implemented on the programmable FPGA chip 388  
 351 of the flash ADC. The algorithm performs a search of the peak 389

of the signal pulse and determines the time from the shape of the leading edge of the pulse. The times of all hits constituting the CCAL shower are combined to form the shower time by using an energy-weighted sum. The time difference between beam photon candidates and CCAL showers originating from Compton events is presented in Fig. 13. The main peak on this plot corresponds to beam photons and CCAL clusters produced in the same accelerator bunch. Satellite peaks, separated by the beam bunch period of about 4 ns, represent accidental beam photons from accelerator bunches not associated with the interaction in the detector. The time resolution of CCAL showers is improved with the increase of the shower energy and was measured to be about 330 ps and 140 ps for 1 GeV and 9 GeV showers, respectively. In the PrimEx  $\eta$  experiment, the CCAL allowed a clear separation of beam photons originating from different beam bunches.

Reconstruction of electromagnetic showers in the FCAL is performed using an algorithm described in Ref. [21], which is a part of the standard GlueX reconstruction software. For the CCAL, we implemented an algorithm originally developed for the GAMS spectrometer [22, 23], which was subsequently adopted for the HyCal [13] in JLab's experimental Hall B. The algorithm provides a good separation of overlapping showers in the calorimeter by using profiles of electromagnetic showers. The elasticity distribution, defined as the reconstructed energy in the event minus the beam energy, is presented in Fig. 14 for Compton candidates produced by beam photons in the energy range between 6 GeV and 7 GeV. The solid line shows the fit of this distribution to the sum of a Gaussian and a second order polynomial function. The energy resolution of reconstructed Compton candidates in this energy range is about 130 MeV. In this plot, we subtracted background originating from accidental beam photons. This background was measured using off-time interactions and amounted to about 15%. The relatively small background, on the level of 10%, produced by interactions of the photon beam with the beamline material downstream the GlueX target was measured using empty-target runs and was also excluded from the elasticity distribution in Fig. 14. The

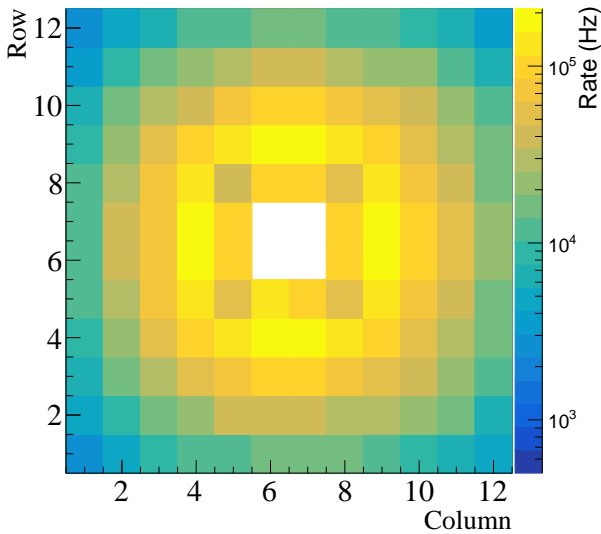


Figure 12: Rates in the CCAL modules during PrimEx  $\eta$  production run. The energy threshold corresponds to 30 MeV. The beam goes through the center of the hole in the middle of the plot.

CCAL allowed to clearly reconstruct Compton events in the PrimEx  $\eta$  experiment.

#### 4. Upgrade of the GlueX forward calorimeter

The forward calorimeter of the GlueX detector consists of 2800 lead glass modules, each with a size of 4 cm  $\times$  4 cm  $\times$  45 cm, and is positioned about 6 m downstream of the target, as shown in Fig. 1. The FCAL covers a polar angle of photons produced from the target between 1° and 11° and detects showers with energies in the range of 0.1 - 8 GeV. The Cherenkov light produced in the module is detected by FEU-84-3 photomultiplier tubes, instrumented with Cockcroft-Walton bases [24]. The typical energy resolution of the FCAL is  $\sigma_E/E = 6.2\%/\sqrt{E} \oplus 4.7\%$ .

The future physics program with the GlueX detector in Hall D will require an upgrade of the inner part of the forward calorimeter with high-granularity, high-resolution PbWO<sub>4</sub> crystals. The lead tungstate insert will improve the separation of clusters in the forward direction and the energy resolution of reconstructed photons by about a factor of two. Lead tungstate crystals possess better radiation hardness compared to lead glass, which is important for the long term operation of the detector at high luminosity. The size of the insert will tentatively comprise 1596 PbWO<sub>4</sub> crystals, which will form an array of 40  $\times$  40 modules<sup>5</sup>. Similar to the CCAL, the insert will have a beam hole of 2  $\times$  2 modules and a tungsten absorber used to cover the detector layer closest to the beamline. A schematic view of the FCAL frame with the installed lead tungstate insert

<sup>5</sup>The insert size proposed for the JEF experiment [2] is 1 m  $\times$  1 m; the actual size will depend on the availability of funds.

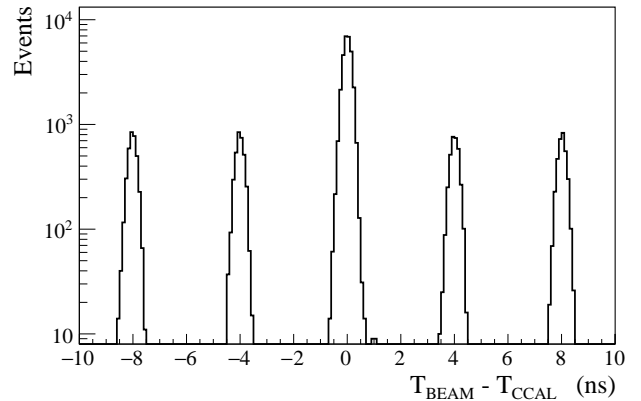


Figure 13: Time difference between beam photons and reconstructed CCAL showers for Compton candidates. Peaks are separated by the beam bunch period of 4 ns.

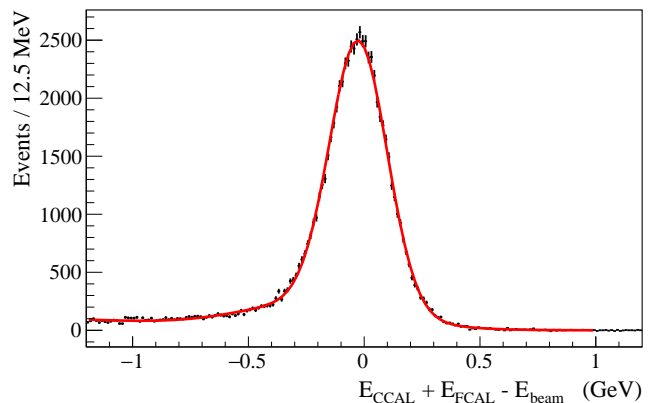


Figure 14: Elasticity distribution of reconstructed Compton candidates.

is presented in Fig. 15. Due to the different size of the lead glass bars and lead tungstate crystals, the lead glass modules stacked around the PbWO<sub>4</sub> insert will form four regions with a relative offset between modules; those regions are shown in green color in this plot.

The PbWO<sub>4</sub> module design of the FCAL insert will essentially be the same as for the CCAL, except for some small modifications needed to handle the magnetic field present in the FCAL region. The PMT housing made of the G-10 fiberglass material will be replaced by iron housing in order to reduce the magnetic field. The housing length will be increased to extend the magnetic shield beyond the PMT photocathode. An acrylic optical light guide will be inserted inside the PMT housing to couple the crystal and PMT.

The upgraded FCAL will be operated in GlueX experiments using a 30 cm long liquid hydrogen target at the designed photon flux of  $5 \cdot 10^7$   $\gamma$ /sec in the energy range between 8.4 GeV and 9 GeV. The designed luminosity is significantly larger than that used in the PrimEx  $\eta$  experiment and was achieved after the PrimEx run in the fall of 2019. In order to finalize the design of the PMT electronics, it is important to understand detector rates

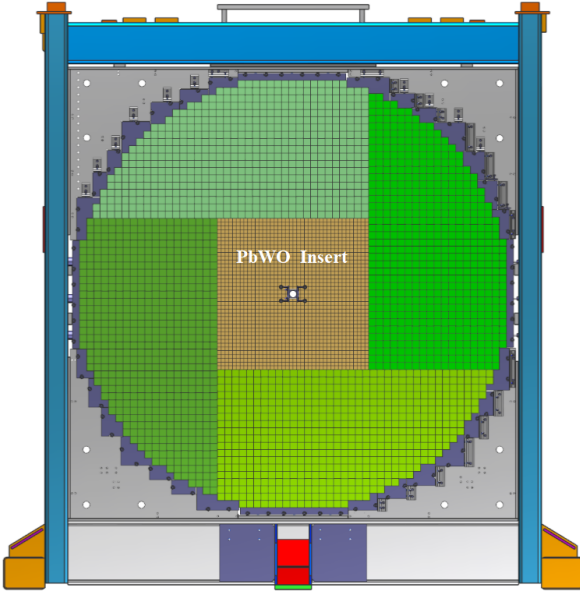


Figure 15: FCAL frame with calorimeter modules installed: PbWO<sub>4</sub> crystals (brown area), lead glass blocks (green). The photon beam passes through the hole in the middle of the calorimeter.

in the FCAL insert, especially in layers close to the beamline. We used the CCAL during high-intensity GlueX runs to study run conditions for the FCAL insert.

#### 4.0.1. Magnetic shielding of PMTs

The longitudinal (directed along the beamline) and transverse (directed perpendicular to the axis of the beamline) components of the magnetic field produced by the GlueX solenoid magnet in the FCAL PbWO<sub>4</sub> insert area vary between 40 - 55 Gauss and 0 - 9 Gauss, respectively. The longitudinal field is the largest on the beamline, where the transverse component is practically absent. We studied the PMT magnetic shielding using a prototype consisting of an array of 3 × 3 PMT iron housings made of AISI 1020 steel, which was positioned in the middle of Helmholtz coils. Each housing had a size of 20.6 mm × 20.6 mm × 104 mm with a 20 mm round hole in the middle for the PMT. This corresponds to the realistic size of the magnetic shield that will be used in the calorimeter module assembly. Inside the housing we inserted two layers of mu-metal cylinders, with thicknesses of 350 μm and 50 μm, separated from each other by a Kapton film. The thickest cylinder was spot welded and annealed.

The Helmholtz coils had a diameter of about 1.5 m and can generate a uniform magnetic field with variable strength below 100 Gauss. A Hall probe was inserted into the central module of the prototype to measure the magnetic field at different Z-positions along the length of the cylinder. The field was measured for two different orientations of the prototype with respect to the magnetic field: field oriented along the PMT (longitudinal,  $B_z$ ) and perpendicular to the PMT housing (transverse,  $B_x$ ). Field measurements are presented in Fig. 16. The PMT shield significantly reduces both the longitudinal and transverse fields to the level of  $B_z \sim 1$  Gauss and  $B_x \ll 1$  Gauss. The

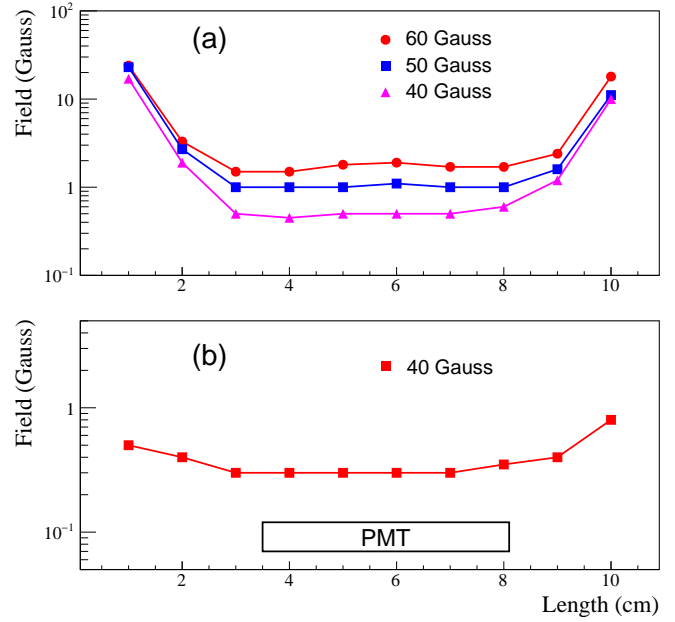


Figure 16: Magnetic field distribution inside the PMT shield housing as a function of the distance from the housing face. Plot (a) corresponds to the longitudinal field and plot (b) corresponds to the transverse field produced by the Helmholtz coils. Markers denote different field values.

transverse field, which is well shielded, is more critical for the PMT operation, as it is directed perpendicular to the electron trajectory inside the photo tube and deflects electrons, resulting in the degradation of the photon detector efficiency and gain. The field reaches a plateau at  $Z = 3$  cm from the face of the housing. We will use 3.5 cm long acrylic light guides, in order to place the most sensitive to the magnetic field area of the PMT between the photocathode and the last dynode (4.6 cm long) in the region with the smallest magnetic field, as shown in Fig. 16. The actual field inside the FCAL insert module is expected to be even smaller due to the collective shielding effect, i.e., the large amount of shielding material installed on surrounding modules [25].

We studied performance of the shielded PMT in the magnetic field using an LED pulser. A blue LED with a light diffuser was placed about 20 cm from the PMT housing prototype and was aligned with the middle module. The PMT response was measured for different pulse amplitudes and operational high voltages. In order to study the contributions from longitudinal and transverse field components we rotated the prototype by different angles. Signal amplitudes as a function of the magnetic field measured in the prototype tilted by about 10 degrees are presented on the top plot of Fig. 17. Amplitudes, normalized to measurements without magnetic field, are shown on the bottom plot. The relative degradation of the signal amplitude for the maximum field in the FCAL insert region of  $B = 55$  Gauss ( $B_z \sim 54$  Gauss and  $B_x \sim 9$  Gauss) was measured to be on the level of 1%. The proposed shielding configuration is sufficient to reduce the magnetic field to the level suitable for the PMT operation.



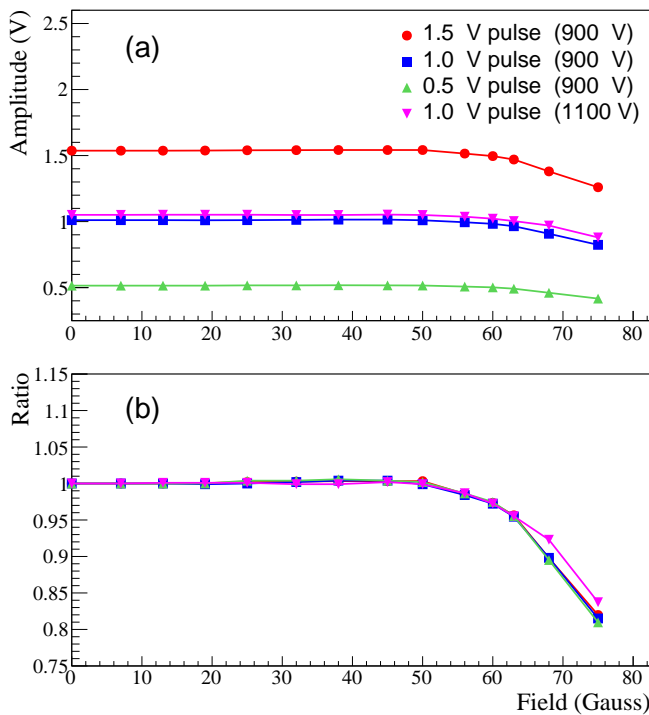


Figure 17: Signal amplitudes of shielded PMT induced by an LED as a function of the magnetic field (a). Amplitudes, normalized to measurements without magnetic field (b). The PMT response was measured for different intensities of light pulse and HV settings as shown by different polymarkers.

#### 4.0.2. Light guide studies

Studies of the magnetic shielding demonstrated that the PMT has to be positioned inside the iron housing at the distance of at least 3 cm from the face of the  $\text{PbWO}_4$  crystal. In order to do this, in the FCAL insert module we decided to use a 3.5 cm long acrylic cylindrical light guide with a diameter of 18.5 mm between the PMT and the  $\text{PbWO}_4$  crystal. The light guide is wrapped with reflective ESR foil and attached to the PMT with Dymax 3094 UV curing glue. Optical coupling to the crystal is provided by a “silicon cookie”: a 1 mm thick transparent rubber cylinder made of the room temperature vulcanized silicon compound, RTV615. The silicon cookie is not glued to the light guide or the crystal, so the module can be easily disassembled if its PMT needs to be replaced.

We compared light losses of the FCAL insert module instrumented with the light guide with the CCAL module, where the PMT was coupled directly to the crystal using an optical grease. Light collection was measured using electrons provided by the Hall D pair spectrometer (PS) [18]. The PS is used to measure the flux of beam photons delivered to the experimental hall by detecting electromagnetic electron-positron pairs produced by the photons in a thin converter inserted to the beam. Leptons from the pair are deflected in a dipole magnet and registered using scintillator detectors placed in the electron and positron arms of the spectrometer. The energy of a lepton is detected using a high-granularity PS hodoscope, which consists of 145

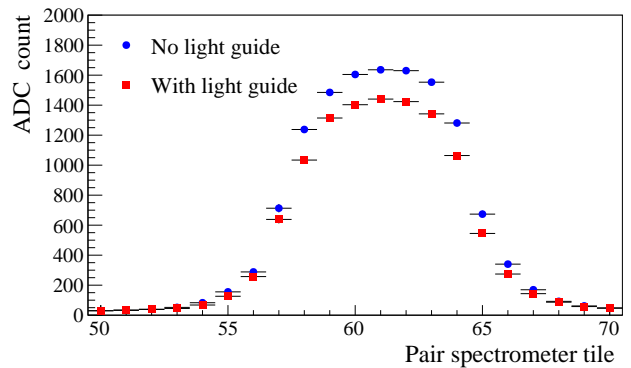


Figure 18: ADC amplitudes of the calorimeter module as a function of the pair spectrometer tile for two configurations: the PMT directly coupled to the  $\text{PbWO}_4$  crystal (circles), and the PMT coupled to the module using an optical light guide (boxes).

scintillating tiles and covers the energy range between 3 GeV and 6 GeV. Each tile corresponds to the specific lepton energy.

The relative light yield of the module with and without the light guide was estimated by positioning the module behind the PS and measuring signal amplitudes induced by the PS electrons. We first measured the ADC response in the CCAL module, which was subsequently modified by adding the light guide to the same PMT and crystal and was placed to the same spot of the PS test setup. Results of the measurements are presented in Fig. 18. The ADC amplitude of the calorimeter module is presented as a function of the PS tile for the two module configurations with and without the light guide. The light guide results in a relatively small loss of light of 15 – 20% compared with the CCAL module. We note that wrapping the light guide with the reflective material is important. Losses in unwrapped light guide constitute about 35%. We repeated light collection measurements using two more modules and obtained consistent results.

#### 4.0.3. Detector rate

The PMT anode current is one of the critical characteristics that have to be considered during the design of the PMT divider. Typically the anode current should be on the level of a few micro amperes and significantly smaller than the divider current in order to provide stable performance of the PMT base and prevent the long-term degradation of the PMT. Some lifetime tests of the Hamamatsu 4125 PMT are described in Ref. [26].

The anode current ( $I$ ) was measured in the CCAL modules during data production runs at the GlueX nominal luminosity. It was obtained by measuring the average voltage in the flash ADC induced by particles incident on the CCAL module as follows:

$$I = \frac{\bar{U}}{R} \cdot \frac{1}{G}, \quad (2)$$

where  $\bar{U}$  is the average voltage in units of Volts,  $R$  is the input impedance of the amplifier ( $\sim 50 \Omega$ ), and  $G$  is the amplifier

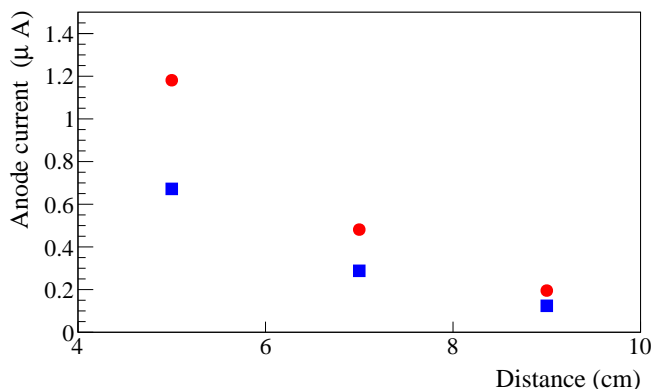


Figure 19: Typical PMT anode current of CCAL modules positioned at different distances from the beamline. Circles correspond to the nominal GlueX luminosity, boxes correspond to 60% of the nominal luminosity.

gain of 24. A periodic pulser not associated with an interaction in the detector was used as a trigger to read out flash ADC raw data for each CCAL module in a time window of 400 ns. The voltage was determined by summing up ADC amplitudes in the readout window and normalizing the sum to the window size. The typical anode current measured in CCAL modules situated at different distances from the beam line is presented in Fig. 19. Modules from the first CCAL layer closest to the beamline and the outer most layer were not used in the analysis. The inner modules were shielded by a tungsten absorber and the outer modules were obscured by the FCAL. The rate in the detector is dominated by the forward-directed electromagnetic background. The estimated anode current is the largest in the innermost layer of the detector closest to the beam line and amounts to about  $1.4 \mu\text{A}$ . This current is significantly smaller than the PMT divider current of about  $300 \mu\text{A}$ .

We used the CCAL measurements to estimate the current in the FCAL insert. Taking the geometrical location of FCAL and CCAL modules into account, the largest PMT current in the FCAL insert modules closest to the beam line was conservatively estimated to be about  $15 \mu\text{A}$ . We assume that the PMT base is operated at 1 kV and no amplifier is used. The detector rate drops rapidly with the increase of the radial distance from the beamline. The anode current is relatively large and must be reduced by lowering the PMT high voltage. We are considering to instrument PMTs in a few inner FCAL insert layers with an amplifier with a gain of 5 and to omit the amplifier on other modules. We are planning to perform more beam tests of the FCAL insert active base using the CCAL in forthcoming GlueX runs in 2021 - 2022.

## 5. Neutral Particle Spectrometer

The NPS is a new facility in Hall C that will allow access to precision measurements of small cross sections of reactions with neutral final states. The NPS consists of an electromagnetic calorimeter preceded by a sweeping magnet. As operated in Hall C, it replaces one of the focusing spectrometers.

The NPS science program currently features six fully approved experiments. E12-13-010 [4] and E12-06-114 [5] experiments will measure the Exclusive Deeply Virtual Compton Scattering and  $\pi^0$  cross sections to the highest  $Q^2$  accessible at Jefferson Lab. Both experiments will provide important information for understanding Generalized Parton Distributions (GPDs). The E12-13-007 [6] experiment will study semi-inclusive  $\pi^0$  electroproduction process and seeks to validate the factorization framework that is needed by the entire 12 GeV Jefferson Lab semi-inclusive deep-inelastic scattering program. Measurements of Wide-Angle and Timelike Compton Scattering reactions will be performed by the E12-14-003 [7] and E12-17-008 [8] experiments. These measurements will allow to test universality of GPDs using high-energy photon beams. The NPS will also be used in the E12-14-005 [9] experiment to study exclusive production of  $\pi^0$  at large momentum transfers in the process  $\gamma p \rightarrow \pi^0 p$ .

The NPS science program requires neutral particle detection over an angular range between 6 and 57.3 degrees at distances of between 3 and 11 meters<sup>6</sup> from the experimental target. The experiments will use a high-intensity beam of electrons with the energies of 6.6, 8.8, and 11 GeV, and a typical luminosity of  $\sim 10^{38} \text{ cm}^{-2}\text{s}^{-1}$  as well as a secondary beam of photons incident on a liquid hydrogen target. A vertical-bend sweeping magnet with integrated field strength of 0.3 Tm will be installed in front of the spectrometer in order to suppress and eliminate background of charged particle tracks originating from the target. The photon detection is the limiting factor of the experiments. Exclusivity of the reaction is ensured by the missing mass technique and the missing-mass resolution is dominated by the energy resolution of the calorimeter. The calorimeter is anticipated to provide the spacial resolution of 2-3 mm and the energy resolution of about  $2.5\% / \sqrt{E}$ . The NPS consists of 1080  $\text{PbWO}_4$  crystals that form an array of  $30 \times 36$  modules. Similarly to the FCAL insert in Hall D, the NPS will be built from the crystals of the same size, and instrumented with the same type of PMTs and readout electronics. The details of the mechanical assembly and commissioning of the NPS are currently under development and will be described in a forthcoming publication.

The radiation hardness and good optical quality of lead tungstate crystals are critical for the NPS calorimeter. The NPS collaboration, in a synergistic effort with the EIC eRD1 consortium, has characterized to date over 1200  $\text{PbWO}_4$  crystals produced by CRYTUR and SICCAS from 2014 to the present. The results of these studies have been published in Ref. [10]. CRYTUR crystal samples were found to have greater overall uniformity in transmittance and light yield, and better radiation hardness. Of the samples characterized by the NPS collaboration 140 SICCAS crystals have been used in the CCAL detector.

## 6. Summary

We described the design and performance of the Compton calorimeter, which was constructed using 140 lead tungstate

<sup>6</sup>The minimum NPS angle at 3 m is 8.5 degrees; at 4 m it is 6 degrees.

PbWO<sub>4</sub> crystals recently produced by SICCAS. The calorimeter was successfully used in the PrimEx  $\eta$  experiment in spring of 2019 for reconstruction of Compton scattering events. The CCAL served as a prototype for two large-scale electromagnetic calorimeters based on the PbWO<sub>4</sub> crystals: the lead tungstate insert of the forward calorimeter of the GlueX detector and the neutral particle spectrometer. Experience gained during construction and operation of the CCAL provided important information for finalizing the design of FCAL PbWO<sub>4</sub> modules and PMT dividers and also served to further optimize the NPS calorimeter. We presented the design of the FCAL lead tungstate insert and gave an overview of the NPS project.

## 7. Acknowledgments

This work was supported by the Department of Energy. Jefferson Science Associates, LLC operated Thomas Jefferson National Accelerator Facility for the United States Department of Energy under contract DE-AC05-06OR23177. This work was supported in part by NSF grants PHY1714133 and PHY2012430. We thank the NPS collaboration/project for providing PbWO<sub>4</sub> crystals and PMTs used in the construction of the CCAL.

## References

[1] S. Adhikari, et al., The GLUEX beamline and detector, Nucl. Instrum. Meth. A 987 (2021) 164807. [arXiv:2005.14272](https://arxiv.org/abs/2005.14272), doi:10.1016/j.nima.2020.164807.

[2] JLab Experiment **E12-12-002**, Eta Decays with Emphasis on Rare Neutral Modes: The JLab Eta Factory (JEF) Experiment, available online: [https://www.jlab.org/exp\\_prog/proposals/14/PR12-14-004.pdf](https://www.jlab.org/exp_prog/proposals/14/PR12-14-004.pdf).

[3] T. Horn, et al., Scintillating crystals for the Neutral Particle Spectrometer in Hall C at JLab, Nucl. Instrum. Meth. A 956 (2020) 163375. [arXiv:1911.11577](https://arxiv.org/abs/1911.11577), doi:10.1016/j.nima.2019.163375.

[4] JLab experiment **E12-13-010**, Exclusive Deeply Virtual Compton and Neutral Pion Cross-Section Measurements in Hall C, available online: [https://www.jlab.org/exp\\_prog/proposals/13/PR12-13-010.pdf](https://www.jlab.org/exp_prog/proposals/13/PR12-13-010.pdf).

[5] JLab experiment **E12-06-114**, Measurements of the Electron-Helicity Dependent Cross Sections of Deeply Virtual Compton Scattering with CEBAF at 12 GeV, available online: [https://www.jlab.org/exp\\_prog/proposals/06/PR12-06-114.pdf](https://www.jlab.org/exp_prog/proposals/06/PR12-06-114.pdf).

[6] JLab experiment **E12-13-007**, Measurement of SemiInclusive  $\pi^0$  Production as Validation of Factorization, available online: [https://www.jlab.org/exp\\_prog/proposals/13/PR12-13-007.pdf](https://www.jlab.org/exp_prog/proposals/13/PR12-13-007.pdf).

[7] JLab experiment **E12-14-003**, Wide-angle Compton Scattering at 8 and 10 GeV Photon Energies, available online: [https://www.jlab.org/exp\\_prog/proposals/14/PR12-14-003.pdf](https://www.jlab.org/exp_prog/proposals/14/PR12-14-003.pdf).

[8] JLab experiment **E12-17-008**, Polarization Observables in Wide-Angle Compton Scattering at large  $s$ ,  $t$ , and  $u$ , available online: [https://www.jlab.org/exp\\_prog/proposals/17/PR12-17-008.pdf](https://www.jlab.org/exp_prog/proposals/17/PR12-17-008.pdf).

[9] JLab experiment **E12-14-005**, Wide Angle, Exclusive Photoproduction of  $\pi^0$  Mesons, available online: [https://www.jlab.org/exp\\_prog/proposals/14/PR12-14-005.pdf](https://www.jlab.org/exp_prog/proposals/14/PR12-14-005.pdf).

[10] T. Horn, et al., Scintillating crystals for the Neutral Particle Spectrometer in Hall C at JLab, Nucl. Instrum. Meth. A 956 (2020) 163375. [arXiv:1911.11577](https://arxiv.org/abs/1911.11577), doi:10.1016/j.nima.2019.163375.

[11] R. Abdul Khalek, et al., Science Requirements and Detector Concepts for the Electron-Ion Collider: EIC Yellow Report [arXiv:2103.05419](https://arxiv.org/abs/2103.05419).

[12] JLab Experiment **E12-10-011**, A Precision Measurement of the  $\eta$  Radiative Decay Width via the Primakoff Effect, available online: [https://www.jlab.org/exp\\_prog/proposals/10/PR12-10-011.pdf](https://www.jlab.org/exp_prog/proposals/10/PR12-10-011.pdf).

[13] M. Kubantsev, I. Larin, A. Gasparian, Performance of the PrimEx electromagnetic calorimeter, AIP Conf. Proc. 867 (1) (2006) 51–58. [arXiv:physics/0609201](https://arxiv.org/abs/physics/0609201), doi:10.1063/1.2396938.

[14] A. Gasparian, A high performance hybrid electromagnetic calorimeter at Jefferson Lab, in: 11th International Conference on Calorimetry in High-Energy Physics (Calor 2004), 2004.

[15] V. Popov, H. Mkrtchyan, New photomultiplier active base for hall c jefferson lab lead tungstate calorimeter, in: 2012 IEEE Nuclear Science Symposium and Medical Imaging Conference Record (NSS/MIC), 2012, pp. 1177–1179. doi:10.1109/NSSMIC.2012.6551294.

[16] F. Barbosa, et al., A VME64x, 16-Channel, Pipelined 250 MSPS Flash ADC With Switched Serial (VXS) Extension, Tech. rep., Jefferson Lab, Technical Report GlueX-doc-1022 (hyperlink) (Apr. 2007).

[17] R. Brun, F. Rademakers, ROOT: An object oriented data analysis framework, Nucl. Instrum. Meth. A 389 (1997) 81–86. doi:10.1016/S0168-9002(97)00048-X.

[18] F. Barbosa, C. Hutton, A. Sitnikov, A. Somov, S. Somov, I. Tolstukhin, Pair spectrometer hodoscope for Hall D at Jefferson Lab, Nucl. Instrum. Meth. A 795 (2015) 376–380. doi:10.1016/j.nima.2015.06.012.

[19] A. Somov, Development of level-1 triggers for experiments at Jefferson Lab, AIP Conf. Proc. 1560 (1) (2013) 700–702. doi:10.1063/1.4826876.

[20] F. Barbosa, et al., Characterization of the NPS and CCAL readout, Tech. rep., Jefferson Lab, GlueX-doc-3272, (2017), <https://halldweb.jlab.org/doc-public/DocDB/ShowDocument?docid=3272>.

[21] R. T. Jones, et al., A bootstrap method for gain calibration and resolution determination of a lead-glass calorimeter, Nucl. Instrum. Meth. A 566 (2006) 366–374. doi:10.1016/j.nima.2006.07.061.

[22] A. Lednev, Separation of the overlapping electromagnetic showers in the cellular gams-type calorimeters., Tech. rep., IHEP Protvino, Preprint IHEP (1993) 93-153.

[23] F. Binon, et al., Hodoscope multi-photon spectrometer GAMS-2000, Nucl. Instrum. Meth. A 248 (1986) 86. doi:10.1016/0168-9002(86)90501-2.

[24] A. Brunner, et al., A Cockcroft-Walton base for the FEU84-3 photomultiplier tube, Nucl. Instrum. Meth. A 414 (1998) 466–476. doi:10.1016/S0168-9002(98)00651-2.

[25] O. Glamazdin, TOSCA simulation of the magnetic shielding of the FCAL insert, Tech. rep., Jefferson Lab, GlueX-doc-3561, (2018), <https://halldweb.jlab.org/doc-private/DocDB/ShowDocument?docid=3561>.

[26] W. Koska, S. W. Delchamps, J. Freeman, W. Kinney, D. Lewis, P. Limon, J. Strait, I. Fiori, M. Gallinaro, Q. Shen, Evaluation of candidate photomultiplier tubes for the upgrade of the CDF end plug calorimeter, Nucl. Instrum. Meth. A 406 (1998) 103–116. doi:10.1016/S0168-9002(97)01193-5.